AUTOPHAGY
2021, VOL. 17, NO. 6, 1379–1392
https://doi.org/10.1080/15548627.2020.1761653

Taylor & Francis
Taylor & Francis Group

RESEARCH PAPER

Selective autophagy controls the stability of transcription factor IRF3 to balance type I interferon production and immune suppression

Yaoxing Wu[a], Shouheng Jin[a], Qingxiang Liu[a], Yu Zhang[a], Ling Ma[a], Zhiyao Zhao[a], Shuai Yang[a], Yi-Ping Li[b,c], and Jun Cui [a]

[a]State Key Laboratory of Oncology in South China, MOE Key Laboratory of Gene Function and Regulation, School of Life Sciences, Sun Yat-sen University, Guangzhou, GD, China; [b]Institute of Human Virology, Zhongshan School of Medicine, and Key Laboratory of Tropical Diseases Control Ministry of Education, Sun Yat-sen University, Guangzhou, GD, China; [c]Department of Infectious Disease, The Fifth Affiliated Hospital of Sun Yat-sen University, Zhuhai, GD, China

ABSTRACT

IRF3 (interferon regulatory factor 3) is one of the most critical transcription factors in antiviral innate immune signaling, which is ubiquitously expressed in a variety of cells. Although it has been demonstrated that IRF3 can provoke multiple cellular processes during viral infection, including type I interferon (IFN) production, the mechanisms underlying the precise regulation of IRF3 activity are still not completely understood. Here, we report that selective macroautophagy/autophagy mediated by cargo receptor CALCOCO2/NDP52 promotes the degradation of IRF3 in a virus load-dependent manner. Deubiquitinase PSMD14/POH1 prevents IRF3 from autophagic degradation by cleaving the K27-linked poly-ubiquitin chains at lysine 313 on IRF3 to maintain its basal level and IRF3-mediated type I IFN activation. The autophagic degradation of IRF3 mediated by PSMD14 or CALCOCO2 ensures the precise control of IRF3 activity and fine-tunes the immune response against viral infection. Our study reveals the regulatory role of PSMD14 in balancing IRF3-centered IFN activation with immune suppression and provides insights into the crosstalk between selective autophagy and type I IFN signaling.

Abbreviations: ATG5: autophagy related gene 5; Baf A_1: bafilomycin A_1; BECN1: beclin 1; CALCOCO2/NDP52: calcium binding and coiled-coil domain 2; CGAS: cyclic GMP-AMP synthase; DDX58/RIG-I: DExD/H-box helicase 58; DUBs: deubiquitinating enzymes; IFN: interferon; IRF3: interferon regulatory factor 3; MAVS: mitochondrial antiviral signaling protein; MOI: multiplicity of infection; PAMPs: pathogen-associated molecule patterns; PBMC: peripheral blood mononuclear cell; PSMD14/POH1: proteasome 26S subunit, non-ATPase 14; RIPA: RLR-induced IRF3-mediated pathway of apoptosis; SeV: Sendai virus; SQSTM1/p62: sequestosome 1; STING1: stimulator of interferon response cGAMP interactor 1; TBK1: TANK binding kinase 1; Ub: ubiquitin; WT: wild type

ARTICLE HISTORY
Received 22 November 2021
Revised 17 April 2021
Accepted 23 April 2021

KEYWORDS
Antiviral immunity; deubiquitination; immune suppression; selective autophagy; type I interferon signaling

Introduction

The innate immune system provides the first line of host defense against invading microorganisms through dynamic protein signaling networks [1]. Pattern recognition receptors (PRRs), including Toll-like receptors (TLRs), RIG-I-like receptors (RLRs), NOD-like receptors (NLRs), and several nucleic acid sensors, initiate the innate antiviral immune responses by detecting viral RNA or DNA [2]. After recognizing the virus-specific features, PRRs hierarchically trigger the signaling cascades, which include adaptor proteins (TICAM1/TRIF, MYD88, MAVS, and STING1), a set of well-studied serine/threonine kinases (IKBKB/IκB kinase complex, TBK1 and IKBKE) and several transcription factors (NFKB/NF-κB, IRF3 and IRF7) [3], to turn on the transcription of type I interferon (IFN) and pro-inflammatory cytokines genes, thus establishing the innate immune state against invading microbes [4].

IRF3 (interferon regulatory factor 3) serves as an indispensable transcription factor for type I IFN production. After receiving upstream signals, IRF3 goes through diverse processes to activate the type I IFN signaling, including phosphorylation, dimerization, translocation to nucleus and stimulation of DNA binding and transcriptional activity of type I IFN genes [5]. The activation of IRF3 mainly depends on the phosphorylation level of IRF3 on its C-terminal phosphorylation clusters. The substitution of alanine (A) for the serine/threonine (S/T) residues from either cluster of IRF3 impairs its activation [6,7]. In addition, IRF3 serves as a pro-apoptotic factor in the late phase of viral infection, which triggers the RLR-induced IRF3-mediated pathway of apoptosis (RIPA) and eliminates the infected cells and invading microbes [8].

In recent decades, extensive studies have focused on the mechanisms underlying the phosphorylation-triggered activation of IRF3 [9]. Meanwhile, the latest research also demonstrated that ubiquitination participates in the regulation of IRF3-dependent type I IFN signaling. The ubiquitin E3 ligases TRIM21, CBL, UBE3 C, RBCK1, PIN1 and FOXO1 are documented to affect the ubiquitination of IRF3 and facilitate its proteasome-dependent degradation, thus negatively regulating type I IFN signaling [10–16]. On the contrary, E2-conjugating enzyme UBE2D1 is required for the K63-linked

CONTACT Jun Cui cuij5@mail.sysu.edu.cn School of Life Sciences, Sun Yat-sen University, 132 Waihuan East Road, Guangzhou, GD 510006, China
Supplemental data for this article can be accessed here.

ubiquitination of IRF3 during viral infection to activate IRF3 [17]. In addition, linear ubiquitin chain assembly complex (LUBAC) mediates the linear polyubiquitination of IRF3 to induce virus-triggered apoptotic cell death [8]. In particular, autophagy is also reported to be involved in the regulation of IRF3 stability [18,19]. However, the detailed mechanisms underpinning the autophagic degradation of IRF3 remain poorly understood.

Macroautophagy, hereafter referred to as autophagy, is a highly conserved eukaryotic degradation process, involving the cellular recycling of multiple cytoplasmic components during physiological conditions, as well as in response to various stresses [20]. Autophagy is highly selective when delivering substrates, such as protein aggregates and damaged or superfluous organelles, to autophagosomes for lysosome degradation via a number of cargo receptors [21]. SQSTM1/p62 (sequestosome 1), CALCOCO2/NDP52 (calcium binding and coiled-coil domain 2), OPTN (optineurin), and NBR1 (next to BRCA1 gene 1 protein) are well-known autophagy cargo receptors that harbor both ubiquitin-binding domains (UBDs) and LC3-interacting regions (LIRs) to ensure the capture of ubiquitinated substrates to autophagosomes [22]. Selective autophagy targets a series of immune factors, such as DDX58, CGAS, MAVS, and STING1, for degradation, thus negatively regulating the activation of the antiviral immune responses [23–26], which implies that selective autophagy suppresses the activation of type I IFN signaling during viral infection. However, the molecular mechanisms underlying the multilayer regulation of selective autophagy in antiviral immune responses and the involvement of autophagy in the precise control of IRF3-based type I IFN signaling remain largely elusive.

In this study, we report that the deubiquitinase PSMD14 (also referred to as Rpn11 or POH1) is required for the activation of innate antiviral immune responses by targeting IRF3. Upon viral infection, PSMD14 disassociates with IRF3, and IRF3 then can be conjugated with K27-linked ubiquitin chains and goes through autophagic degradation in a CALCOCO2-dependent manner, which leads to immune suppression. PSMD14 decreases the K27-linked ubiquitination of IRF3 at K313 to suppress its recognition by CALCOCO2, which subsequently maintains the basal level of IRF3 to ensure the activation of type I IFN signaling. Our findings demonstrate that PSMD14 functions as a positive regulator of innate antiviral immunity to amplify type I IFN signaling and provide insights of the crosstalk between type I IFN signaling and selective autophagy.

Results

Viral infection induces the degradation of IRF3

To investigate the dynamic pattern of IRF3 protein after viral infection, A549 cells were infected with Sendai virus (SeV) at different time points. In the early time point (0–12 h), the protein level of IRF3 did not show a remarkable change, while at the late stage of SeV infection (after 24 h), IRF3 protein level was reduced (Figure 1A and S1A). To confirm the SeV-induced downregulation of IRF3 in immune cells, we detected the protein level of IRF3 in THP-1 cells (a human monocyte cell line) and peripheral blood mononuclear cells (PBMCs) after SeV infection, and also found a downregulation of IRF3 at the late stage of viral infection (Figure 1B, S1B,C).

TBK1 is reported to function as one of the critical kinases of IRF3, and it can associate with IRF3 upon viral infection. In order to detect whether other key molecules in type I IFN signaling pathway could also undergo reduction as IRF3 after viral infection, we used TBK1 as a control. We found the reduction of TBK1 by viral infection is minor, compared to the reduction of IRF3 (Figure S1A,C). By detecting IRF3 protein level after SeV infection with different multiplicities of infection (MOI) (Figure 1A,C), we showed that both lower titer (MOI = 0.03) and higher titer (MOI = 0.1) of virus led to a similar reduction of IRF3 in the late time point during infection. In order to determine the relationship between viral load and IRF3 degradation, we determined the intracellular viral concentration by detecting the RNA level of *SeV phosphoprotein* (Figure S1D). Interestingly, we found the relative protein level of IRF3 exhibited a negative correlation with the intracellular viral concentration (Figure S1E). We further detected the protein level of IRF3 in A549 cells treated with different titers of SeV at both early stage (8 h) and later stage (24 h). Consistently, higher viral load could also induce the decrease of IRF3 protein level even at the early stage (8 h) during viral infection (Figure 1D, E, S1F,G). Additionally, we also confirmed that treatment with intracellular (IC) poly (I:C) (low molecular weight), a ligand of DDX58, could also lead to a concentration-dependent reduction of the protein level of IRF3 at the late stage (24 h) post-poly (I:C) treatment (Figure 1F and S1H).

To rule out the possibility that the decrease of IRF3 protein level was due to its change at transcription level, we found the mRNA abundance of *IRF3* did not show significant differences after viral infection (Figure S1I). To exclude the possibility that the downregulation of IRF3 protein was caused by virus-induced cell death, we analyzed cell viability after viral infection and found that low virus titer did not affect virus-induced cell death (0–48 or −72 h), while higher virus titer (MOI = 10) could cause significant cell death, which is consistent with previous study [8] (Figure S1J,K). Collectively, these results suggest that viral infection leads to the reduction of IRF3 protein in a virus load-dependent manner.

IRF3 undergoes autophagic degradation during viral infection

To determine which degradation system dominantly controls the degradation of IRF3 during viral infection, we detected whether IRF3 degradation could be abrogated by the proteasome inhibitors or the autophagy inhibitors. We found the degradation of IRF3 could be blocked by autophagy and autolysosome inhibitors, such as 3-methyladenine (3-MA), chloroquine (CQ), and bafilomycin A_1 (Baf A_1), but not the proteasome inhibitor MG132, lactacystin, or carfilzomib, indicating that long-term viral infection might result in the autophagic degradation of IRF3 (Figure 1G and S1L). In addition, we observed that the virus-triggered degradation of IRF3 could be inhibited by a nuclear export inhibitor leptomycin B (LMB), which has been reported to impair BECN1 function by blockading its nuclear export [27] (Figure S1 M).

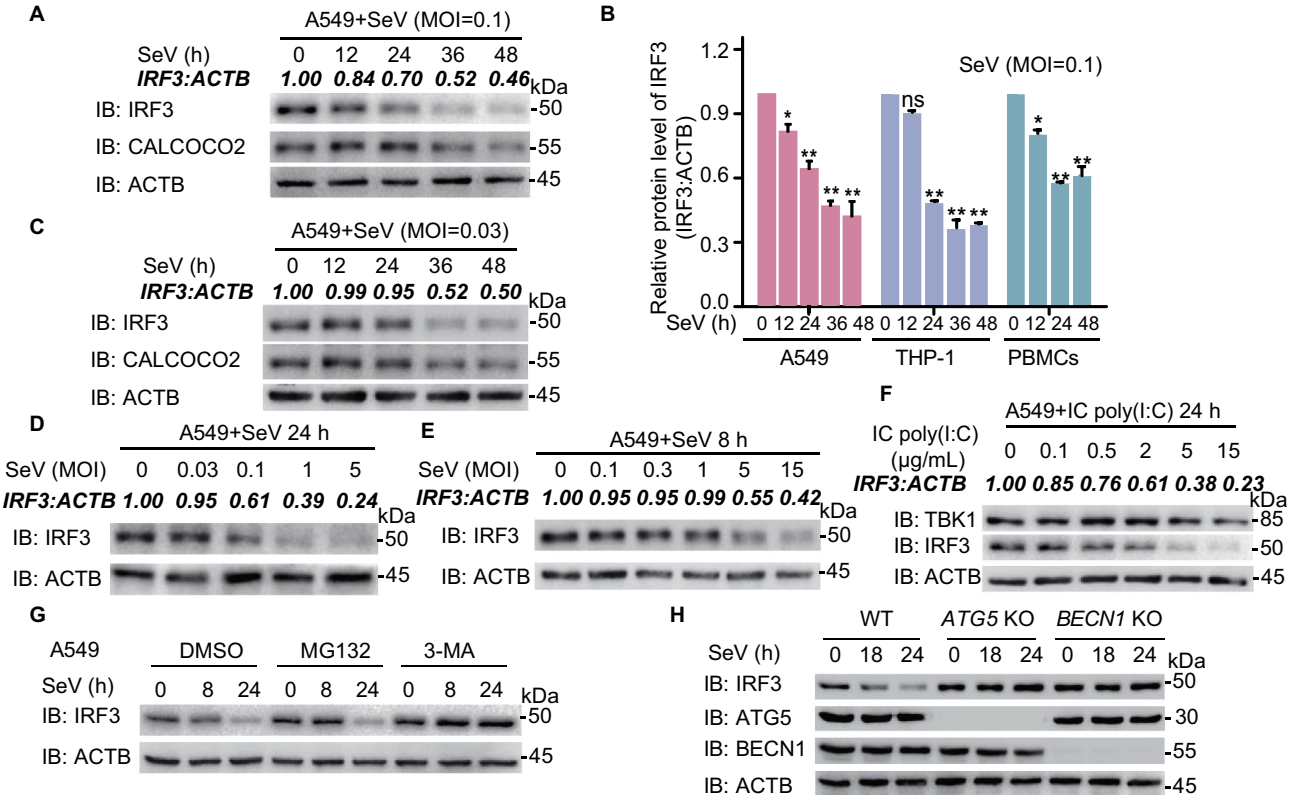

Figure 1. Viral infection induces the autophagic degradation of IRF3. (A) A549 cells were infected with SeV (MOI = 0.1) for indicated time points, and the lysates were harvested for immunoblot analysis. (B) Quantification of the protein level of IRF3 after SeV infection (MOI = 0.1) in A549 cells, THP-1 cells or PBMCs. (C) A549 cells infected with SeV (MOI = 0.03) for indicated time points and the lysates were harvested for immunoblot analysis. (D, E) A549 cells were infected with SeV at indicated MOI for 24 h (D) or 8 h (E), and the lysates were harvested for immunoblot analysis. (F) A549 cells were stimulated with intracellular (IC) poly (I:C) for indicated concentrations for 24 h, and the lysates were harvested for detecting the protein level of IRF3. (G) A549 cells were infected with SeV (MOI = 0.1) for indicated time points, followed with MG132 (10 μM), or 3-methyladenine (3-MA; 10 mM) treatment for 6 h before being harvested. The cell lysates were analyzed by immunoblot. (H) Wild-type (WT), *ATG5* and *BECN1* knockout (KO) 293 T cells were infected with SeV (MOI = 0.1) for 0 h, 18 h or 24 h, and the lysates were analyzed with indicated antibodies. Data in (B) are expressed as mean ± SEM of three independent experiments. *$p < 0.05$, **$p < 0.01$; NS, not significant (two-tailed Student's *t*-test). All other experiments are representatives of three independent biological experiments with similar results.

To exclude the possibility that the rescue of IRF3 reduction was due to the decrease of viral infection, we detected SeV RNA level after treatment of inhibitors such as MG132 and 3-MA. 6 h-treatment of both inhibitors before harvested did not significantly affect the SeV RNA level after 24 h-viral infection (Figure S1N). IRF3 protein level showed a negative correlation with viral concentration after the treatment of DMSO or MG132, but not 3-MA (Figure S1O). To confirm whether IRF3 underwent autophagic degradation after viral infection, we detected the protein level of IRF3 in *BECN1* and *ATG5* knockout (KO) cells, in which autophagy is greatly impaired. As *BECN1* and *ATG5* KO might lead to the reduction of SeV infection, we reduced the MOI of SeV in wild type (WT) cells to balance the replication level of SeV in different cells (Figure S1P). Consistently, the virus-induced reduction of IRF3 was inhibited in *BECN1* and *ATG5* KO cells (Figure 1H and S1Q). Together, these data indicated that IRF3 could undergo autophagic degradation during SeV infection.

The K27-linked ubiquitination of IRF3 at K313 is a signal for autophagic degradation via cargo receptor CALCOCO2

Mounting evidence reveals the critical roles of cargo receptors in delivering substrates for selective autophagic degradation [28,29]. Thus, we subsequently investigated which cargo receptor might be responsible for the autophagic degradation of IRF3. Coimmunoprecipitation (Co-IP) assays showed that IRF3 could interact with cargo receptors SQSTM1 and CALCOCO2 during SeV infection (Figure 2A). However, the degradation of IRF3 was inhibited in *CALCOCO2* KO cells, but not in *SQSTM1* KO cells after SeV infection, indicating the essential role of CALCOCO2 in mediating the autophagic degradation of IRF3 after SeV infection (Figure 2B, S2A,B). We further confirmed that the association between IRF3 and CALCOCO2, but not SQSTM1 was enhanced upon viral infection in A549 cells and PBMCs (Figure 2C,D). Moreover, higher titration of virus could also promote the interaction between CALCOCO2 and IRF3 (Figure 2E). The enhanced colocalization of IRF3 and CALCOCO2 was also observed after SeV infection (Figure 2F). In addition, *CALCOCO2* deficiency enhanced the dimerization of IRF3 as well as the translocation of IRF3 from cytosol to nucleus (Figure 2G and S2C). Collectively, our results suggest that CALCOCO2 performs as a cargo receptor in delivering IRF3 to autophagosomes after viral infection.

To determine which domain of CALCOCO2 is essential for the recognition of IRF3, we generated three different domain deletion mutants of CALCOCO2, including an amino-

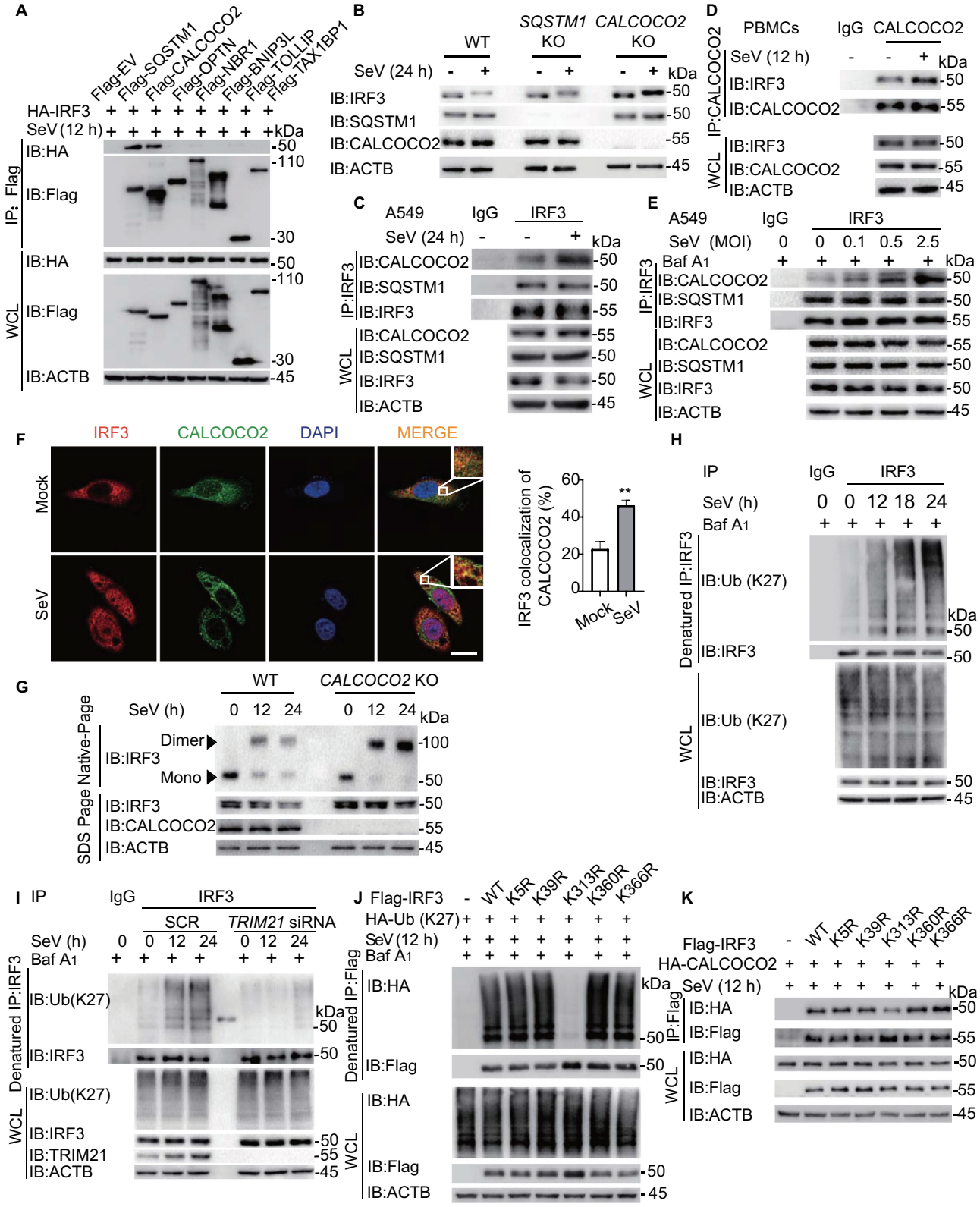

Figure 2. Cargo receptor CALCOCO2 mediates the autophagic degradation of IRF3 with virus-triggered K27-linked ubiquitination. (A) 293 T cells were transfected with vectors encoding HA-IRF3 and indicated Flag-tagged cargo receptors, followed by immunoprecipitation (IP) with anti-Flag beads and immunoblot analysis with anti-HA. (B) Wild type (WT), *SQSTM1* and *CALCOCO2* knockout (KO) 293 T cells were infected with SeV (MOI = 0.1) for 24 h, and the lysates were analyzed with indicated antibodies. (C) Extracts of A549 infected with SeV (MOI = 0.1) for 24 h were subjected to immunoprecipitation with anti-IRF3 and immunoblot analysis with indicated antibodies. (D) Coimmunoprecipitation and immunoblot analysis of PBMCs infected with SeV (MOI = 0.1) for 12 h. (E) Extracts of A549 infected with indicated titration of SeV for 12 h were subjected to immunoprecipitation with anti-IRF3 and immunoblot analysis with indicated antibodies. (F) Confocal microscopy (left) of A549 cells infected with SeV (MOI = 0.1) for 7 h and Baf A_1 (0.2 μM) treatment for 6 h before harvested, followed by labeling of IRF3 and CALCOCO2 with specific primary antibody and an CF568 goat anti-mouse IgG secondary antibody (red) and Alexa Fluor 488 conjugated anti-rabbit-IgG secondary antibody (green). Scale bars, 20 μm. Quantitative analysis (right) of the colocalization (30 cells per sample). Data are expressed as means ± SD of 30 cells. **$p < 0.01$; (two-tailed Student's t-test). (G) WT and *CALCOCO2* KO 293 T cells were infected with SeV (MOI = 0.1) at different time points, and the lysates were analyzed with indicated antibodies. (H) A549 cells were infected with SeV (MOI = 0.1) for indicated time points and protein extracts were harvested after Baf A_1 (0.2 μM) treatment for 6 h.

Protein extracts were immunoprecipitated after 1% SDS denaturation with anti-IRF3 antibody or IgG and analyzed by immunoblot using anti-ubiquitin (Ub; K27-linked) and anti-IRF3 antibodies. (I) A549 cells were transfected with scramble (SCR) or *TRIM21*-specific siRNA, then infected with SeV (MOI = 0.1) for indicated time points and treated with Baf A_1 (0.2 μM) treatment for 6 h before harvested. Protein extracts were immunoprecipitated after SDS denaturation with anti-IRF3 antibody or IgG and analyzed by immunoblot using anti-ubiquitin and anti-IRF3 antibodies. (J) Denature immunoprecipitation and immunoblot analysis of 293 T cells transfected with vectors expressing Flag-IRF3 (WT, K5 R, K39 R, K313 R, K360 R, or K366 R) and HA-K27 Ub mutant (other Ks but not K27 in ubiquitin are replaced by Rs). (K) 293 T cells were transfected with plasmids encoding HA-CALCOCO2 and Flag-IRF3 (WT, K5 R, K39 R, K313 R, K360 R, or K366 R), followed by immunoprecipitation with anti-Flag beads and immunoblot analysis with anti-HA. All the experiments are representatives of three independent biological experiments with similar results.

terminal skeletal muscle and kidney-enriched inositol phosphatase carboxyl homology (SKICH) domain deletion mutant (ΔSKICH), an intermediate CC domain only mutant (CC), and a carboxy-terminal Lin11, Is1-1, and Mec-3 (LIM)-like (LIM-L) domain deletion mutant (ΔLIM-L) (Figure S2D). Compared with WT CALCOCO2, the CC and ΔLIM-L mutants failed to interact with IRF3 after SeV infection (Figure S2E), indicating that the LIM-L domain is necessary for the recognition of IRF3 by CALCOCO2. LIM-L domain of CALCOCO2 contains a Zn finger domain, which is responsible for binding to ubiquitinated substrates, while the K27-linked ubiquitin chain is one of the recognition signals for CALCOCO2 (Figure S2F) [25,30–32]. It is reasonable to assume that ubiquitin chains conjugated to IRF3 after viral infection might serve as a signal for its autophagic degradation. To confirm this assumption, we detected the ubiquitination level of IRF3 after SeV infection and found that SeV infection increased the K27-linked ubiquitination of IRF3 (Figure 2H, S2G,H).

TRIM21 has been reported to be involved in the regulation of both proteasome and autophagy degradation of IRF3 [13,19]. We next investigated whether K27-linked ubiquitination of IRF3 is mediated by TRIM21 after SeV infection and found that *TRIM21* knockdown led to decreased K27-linked ubiquitination of IRF3 and increased IRF3 stability during viral infection (Figure 2I and S2I). To determine the K27-linked ubiquitin binding sites of IRF3, we performed an *in silico* search by UbPred program [33] and identified 5 conservative points of IRF3, containing K5, K39, K313, K360 and K366. Subsequently, we generated the IRF3 mutants in which each potential ubiquitination site was substituted from lysine (K) to arginine (R). Among these mutants, $IRF3^{K313\ R}$ uniquely displayed a reduction in K27-linked ubiquitination after SeV infection (Figure 2J). We also found that TRIM21 failed to facilitate the K27-linked ubiquitination of $IRF3^{K313\ R}$ as well as its virus-induced degradation (Figure S2J). Moreover, the interaction between CALCOCO2 and $IRF3^{K313\ R}$ was attenuated, compared to that with WT IRF3 (Figure 2K). $IRF3^{K313\ R}$ displayed a slower degradation rate compared with WT IRF3 after SeV infection in the "cycloheximide (CHX) chase" assay (Figure S2K).

Given the fact that the murine CALCOCO2 lacks LIM-L domain to recognize ubiquitinated substrates (Figure S2Li) [34,35], we stably overexpressed human CALCOCO2 in RAW264.7 cells (a murine macrophage cell line) (Figure S2Lii). Previous studies revealed that high dose of viral infection led to the degradation of IRF3 in RAW264.7 cells [36], and our results showed that overexpression of human CALCOCO2 in mouse cells could further enhance the virus-triggered degradation of IRF3 at a modest dose of viral infection (Figure S2Liii), which suggested the additional functions of human CALCOCO2. In summary, these results reveal that viral infection can induce the K27-linked ubiquitination of IRF3 at K313 via TRIM21, which subsequently serves as a recognition signal for CALCOCO2 to mediate its autophagic degradation in human cells.

PSMD14 targets IRF3 to promote its stabilization

Ubiquitination can be reversed by deubiquitinating enzymes (DUBs). Considering that viral infection triggered the K27-linked ubiquitination of IRF3, DUBs might also participate in this dynamic process to fine-tune the type I IFN signaling. Based on our recent screening study of 85 DUBs, we detected the potential roles of different DUBs in antiviral immune responses using sgRNA and found that PSMD14 is the only DUB that acts as a positive regulator in type I IFN signaling and functioned at IRF3 level [37]. In order to verify the function of PSMD14, we performed a luciferase reporter assay and found that PSMD14 promoted virus-induced type I IFN activation by targeting IRF3 (Figure S3A,B). To determine the association between PSMD14 and IRF3, we used co-IP and immunoblot analysis and found that PSMD14 showed a stronger binding affinity with IRF3 than with other molecules in the type I IFN signaling pathway (Figure S3C). To further explore the physiological relevance between PSMD14 and IRF3, we examined the endogenous interaction between IRF3 and PSMD14 in A549 cells and PBMCs after SeV infection and revealed that PSMD14 associated with IRF3 in the resting state, while viral infection weakened this association (Figure 3A and S3D). We subsequently investigated how PSMD14 affects IRF3 activity and found that PSMD14 could specifically stabilize IRF3 rather than other molecules in type I IFN signaling pathway (Figure S3E). Knockdown of *PSMD14* in A549 cells resulted in the reduction of endogenous IRF3 both in the resting state and after SeV infection (Figure 3B). Similarly, *PSMD14* deficiency in PBMCs facilitated the degradation of IRF3 both in the resting state and during SeV infection (Figure 3C). Therefore, PSMD14 can target IRF3 and promote the stabilization of IRF3.

To reveal the mechanisms underlying the stabilization of IRF3 mediated by PSMD14, we assessed the IRF3 stability using pharmacologic approaches. The protein level of IRF3 could not be further enhanced by overexpression of PSMD14 after autophagy inhibitor 3-MA and autolysosome inhibitor Baf A_1 treatment, as 3-MA and Baf A_1 treatment reduced the autophagic degradation of IRF3 and led to the saturation of IRF3 level after SeV infection (Figure 3D). Consistently, the virus-triggered reduction of IRF3 was inhibited by overexpressing PSMD14 in WT cell but not in *BECN1* and *ATG5* KO cells

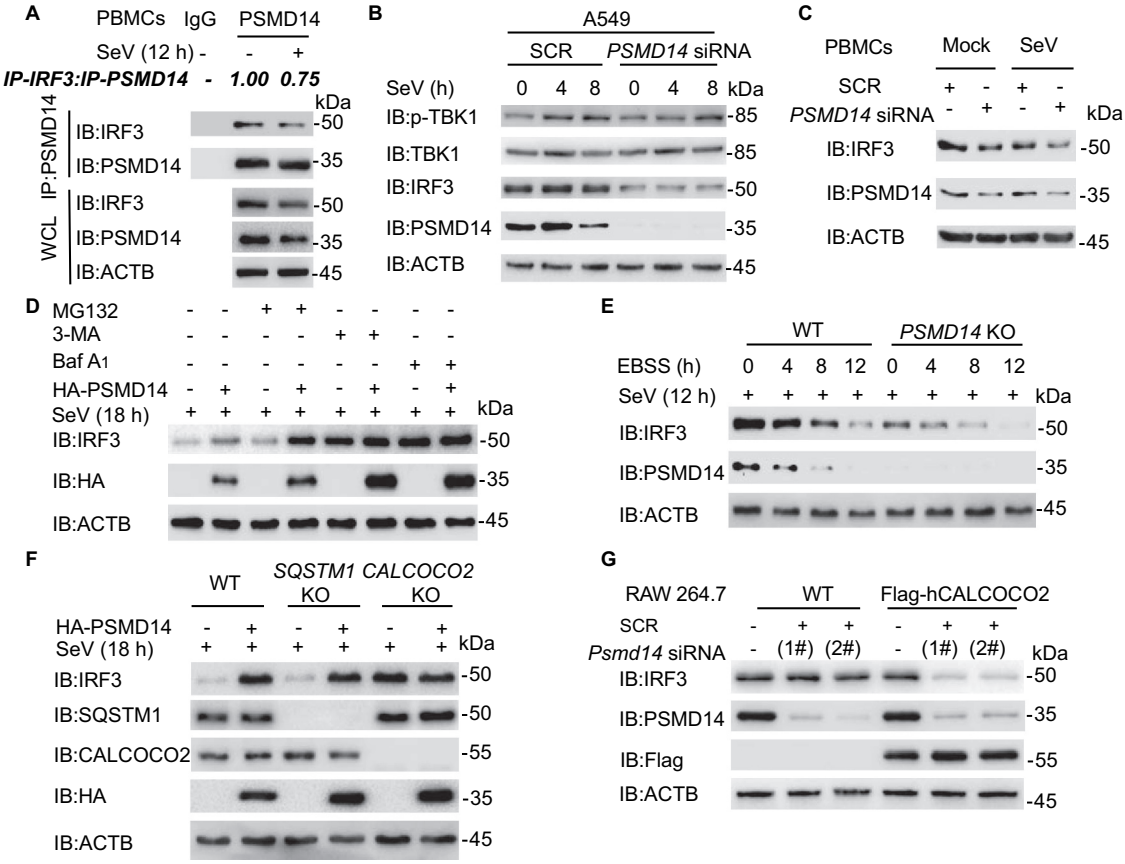

Figure 3. PSMD14 targets IRF3 and promotes its stabilization. (A) Extracts of PBMCs infected with SeV (MOI = 0.1) for indicated time points were subjected to immunoprecipitation with anti-PSMD14 and immunoblot analysis with indicated antibodies. (B) A549 cells were transfected with scramble (SCR) or *PSMD14*-specific siRNA, followed by SeV (MOI = 0.1) infection at different time points, the lysates were analyzed with indicated antibodies. (C) PBMCs were transfected with SCR or *PSMD14*-specific siRNA and treated with SeV (MOI = 0.1) for 24 h. The protein was harvested for immunoblot analysis. (D) 293 T cells were transfected with plasmids encoding Flag-IRF3 together with HA-PSMD14 plasmid and treated with MG132 (10 μM), 3-methyladenine (3-MA; 10 mM), or bafilomycin A_1 (Baf A_1; 0.2 μM) for 6 h before harvest. The cell lysates were analyzed by immunoblot. (E) Wild type (WT) and *PSMD14* knockout (KO) 293 T cells pre-infected by SeV (MOI = 0.1) for 6 h were treated with EBSS for indicated time points. The protein expression level of IRF3 was detected by immunoblot. (F) WT, *SQSTM1* and *CALCOCO2* KO 293 T cells were transfected with plasmid encoding HA-PSMD14, and the lysates were analyzed with indicated antibodies. (G) RAW264.7 cells stably expressing human CALCOCO2 were transfected with SCR or *Psmd14*-specific siRNAs, and the lysates were analyzed with indicated antibodies. All the experiments are representatives of three independent biological experiments with similar results.

(Figure S3F). Moreover, the EBSS-induced autophagic degradation of IRF3 was enhanced in *PSMD14* KO cells (Figure 3E).

As IRF3 could be recognized by CALCOCO2, we speculated that PSMD14 suppressed the CALCOCO2-dependent autophagic degradation of IRF3. As predicted, PSMD14 failed to promote the stabilization of IRF3 in *CALCOCO2* KO cells, but not in *SQSTM1* KO cells (Figure 3F). Moreover, PSMD14 could not affect the protein abundance of $IRF3^{K313\ R}$, which could not be recognized by CALCOCO2 (Figure S3G). We further investigated the function of PSMD14 in murine cells and found that *Psmd14* deficiency could promote the degradation of IRF3 in the presence of human CALCOCO2, but not in WT RAW264.7 cells (Figure 3G). Together, these results indicate that CALCOCO2 specifically controlled the IRF3 stability in human cells, while PSMD14 could reverse this process.

PSMD14 deubiquitinates IRF3

As the K27-linked ubiquitination of IRF3 is essential for its autophagic degradation, we reasoned that PSMD14 might promote the stabilization of IRF3 by removing its K27-linked ubiquitination. We co-expressed different types of ubiquitin mutants together with IRF3 and PSMD14 and found that PSMD14 could specifically cleave the K27-linked ubiquitin chains on IRF3 and displayed low preference for other ubiquitin linkage types on IRF3 (Figure S4A). Furthermore, we found that *PSMD14* depletion led to the enhancement of K27-linked ubiquitination of IRF3 both in the resting state and after SeV infection (Figure 4A). We subsequently generated the catalytically inactive mutants $PSMD14^{C120\ S}$ (CS mutant) and showed that ectopic expression of $PSMD14^{C120\ S}$ failed to remove the K27-linked ubiquitination of IRF3 (Figure S4B). We then reconstituted WT PSMD14 or $PSMD14^{C120\ S}$ in *PSMD14* KO cells and observed that $PSMD14^{C120\ S}$ could barely reduce the virus-triggered K27-linked ubiquitination of IRF3 (Figure 4B). Similarly, *in vitro* deubiquitination assays showed that WT PSMD14 but not $PSMD14^{C120\ S}$ reduced the K27-linked ubiquitin chains of IRF3 (Figure 4C and S4C). In addition, PSMD14 mainly reversed the K27-linked ubiquitination of IRF3 triggered by its E3 ligase TRIM21 (Figure 4D and S4D). We also found

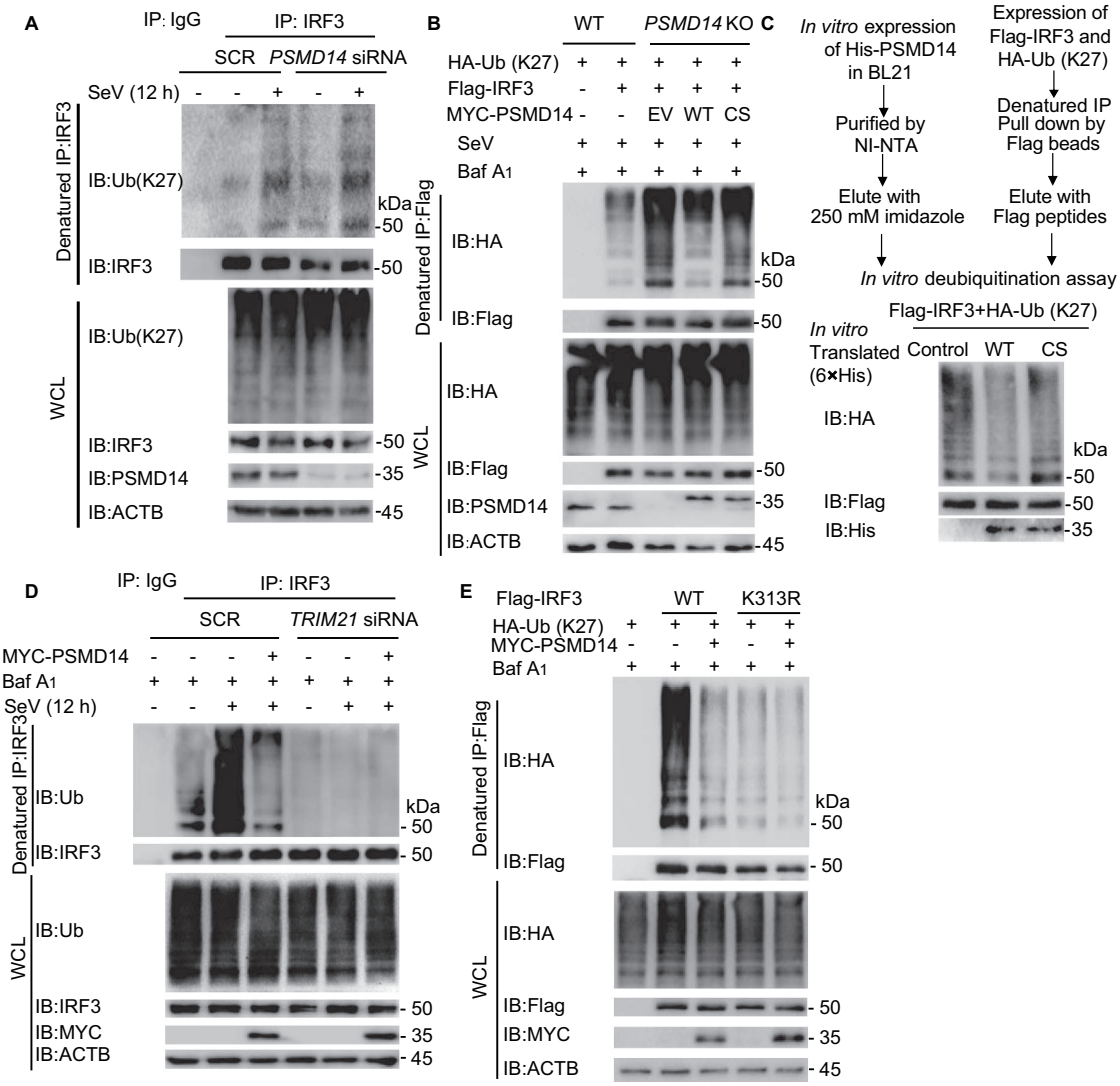

Figure 4. PSMD14 deubiquitinates IRF3 at Lysine 313. (A) A549 cells were transfected with scramble (SCR) or *PSMD14*-specific siRNA, then infected with SeV (MOI = 0.1) for 12 h and protein extracts were harvested after Baf A_1 (0.2 μM) treatment for 6 h. Protein extracts were immunoprecipitated after SDS denaturation with anti-IRF3 antibody or IgG and analyzed by immunoblot using anti-ubiquitin (Ub) and anti-IRF3 antibodies. (B) *PSMD14* knockout (KO) 293 T cells have restored the expression of wild type (WT) or $PSMD14^{C120\ S}$ (CS), then treated with SeV (MOI = 0.1) for indicated time points with Baf A_1 (0.2 μM). The lysates were subjected to SDS denaturation and immunoprecipitation with IRF3 antibody and immunoblot analysis with indicated antibodies. (C) *In vitro* deubiquitination analysis of ubiquitin-modified IRF3 eluted from anti-Flag precipitates by Flag peptide of 293 T cells transfected with Flag-IRF3 and HA-K27-linked-Ub, incubated with PSMD14 or $PSMD14^{C120\ S}$ (CS) obtained from an *in vitro* purification system. (D) 293 T cells were transfected with SCR or *TRIM21*-specific siRNA, together with an empty vector or expression vector for MYC-PSMD14, then infected with SeV (MOI = 0.1) for 12 h. Protein extracts were immunoprecipitated after SDS denaturation with anti-IRF3 and immunoblotted with indicated antibodies. (E) Immunoprecipitation and immunoblot analysis of 293 T cells transfected with vectors expressing Flag-IRF3 WT or Flag-$IRF3^{K313\ R}$ and HA-K27-Ub in the presence of PSMD14. All the experiments are representatives of three independent biological experiments with similar results.

that PSMD14 was not capable of removing the ubiquitin chains on $IRF3^{K313\ R}$ (Figure 4E).

As K27-linked ubiquitin chains function as a recognition signal for CALCOCO2-directed selective autophagy, we further investigated whether the decreased K27-linked ubiquitination of IRF3 induced by PSMD14 affected the IRF3-CALCOCO2 association. We observed that *PSMD14* deficiency enhanced the interaction between IRF3 and CALCOCO2 at the resting state, while this enhancement was alleviated upon viral infection (Figure S4E). Altogether, our results indicated that PSMD14 directly deubiquitinated IRF3 in an enzyme activity-dependent manner, thus suppressing the autophagic degradation of IRF3 through disturbing its recognition by CALCOCO2.

PSMD14 stabilizes the non-phosphorylated IRF3 and maintains the basal expression of IRF3

We next generated several domain mutants of IRF3 (Figure 5A) and found that the IRF association domain (IAD) of IRF3 was indispensable for the association between IRF3 and CALCOCO2 (Figure 5B). As IAD is responsible for mediating the dimerization of IRF3, we hypothesized that PSMD14 could only bind to non-phosphorylated IRF3, but not the active IRF3. To verify this hypothesis, we firstly detected the protein level of IRF3 after SeV infection in *TBK1* KO cells. In the absence of its kinase TBK1, IRF3 could not go through autophagic degradation (Figure 5C). We next performed a two-step immunoprecipitation assay, which separately pulled down the phosphorylated and non-phosphorylated IRF3

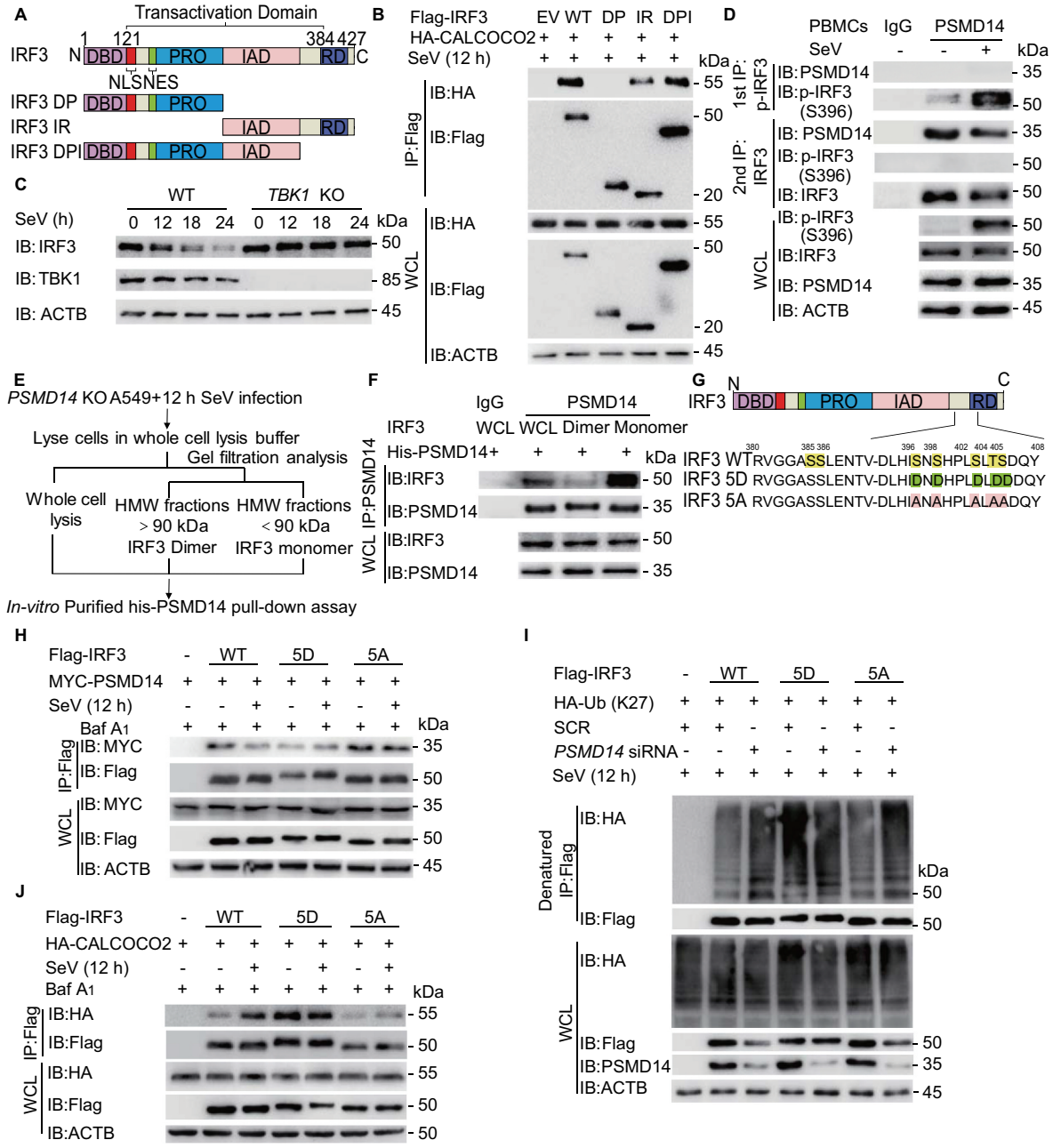

Figure 5. PSMD14 stabilizes the non-phosphorylated IRF3 and maintains the basal level of IRF3. (A) Domain organization of IRF3 protein. (B) Coimmunoprecipitation and immunoblot analysis of 293 T cells transfected with plasmids expressing IRF3 and its indicated mutants along with vector encoding HA-CALCOCO2. (C) Protein lysates of wild type (WT) and *TBK1* knockout (KO) 293 T cells were infected with SeV (MOI = 0.1) for indicated time points were immunoblotted with indicated antibodies. (D) Extracts of human PBMCs infected with SeV (MOI = 0.1) were first subjected to immunoprecipitation with anti-p-IRF3, and the supernatants were subsequently immunoprecipitated by anti-IRF3. All the samples were carried out for immunoblot analysis with indicated antibodies. (E) Experimental setup for the isolation of IRF3 monomer and dimer from *PSMD14* KO A549 cells infected with SeV (MOI = 0.1) for 12 h. (F) Immunoprecipitation and immunoblot analysis of *in vitro* purified his-PSMD14 and whole-cell lysates, IRF3 monomer or dimer from A549 cells after SeV infection for 12 h. (G) The diagrammatic drawing of IRF3 mutants. (H) Immunoblot analysis of protein extracts of 293 T cells transfected with empty vector or vector for MYC-PSMD14, together with plasmid expressing WT, 5D, or 5A mutant of Flag-IRF3 after SeV (MOI = 0.1) infection for 12 h. (I) Denatured immunoprecipitation and immunoblot analysis of 293 T cells transfected with vectors expressing Flag-IRF3 (WT, 5D, or 5A) and HA-K27 ubiquitin mutant in the absence or presence of PSMD14 after SeV infection (MOI = 0.1) for 12 h. (J) 293 T cells were transfected with plasmids encoding HA-CALCOCO2 and Flag-IRF3 (WT, 5D, or 5A) after SeV infection (MOI = 0.1) for 12 h, followed by immunoprecipitation with anti-Flag beads and immunoblot analysis with anti-HA. All the experiments are representatives of three independent biological experiments with similar results.

after viral infection. The IP assay revealed that PSMD14 mainly interacted with the non-phosphorylated IRF3 (Figure 5D and S5A). Given that IRF3 forms dimers after phosphorylation, we separated IRF3 monomers (less than 90 kDa) from dimers (greater than 90 kDa) by gel filtration of SeV-infected *PSMD14* KO A549 cell lysates (Figure 5E), as previously described [38] and showed that *in vitro* purified PSMD14 only interacted with IRF3 monomers but not IRF3 dimers (Figure 5F). Together, our results suggested that PSMD14 selectively associated with non-phosphorylated IRF3 and prevented its K27-linked ubiquitination.

According to previous studies [7,39], IRF3-5D, the phospho-mimetic mutants with the substitution of S/T residues at the C terminal with aspartic acid (D), which discharges the C terminal inhibitory domain of IRF3, led to constitutively

dimerization and activation of IRF3. In contrast, the substitution of these five S/T residues with A greatly impairs the function of IRF3 [40]. We next generated 5D and 5A mutants of IRF3 (Figure 5G), and as expected, we observed that type I IFN signaling was directly activated in IRF3-5D mutant-reconstituted cells, while it was impaired in IRF3-5A mutant-reconstituted cells even after SeV infection or IC poly(I:C) treatment (Figure S5B). By detecting the association between PSMD14 and IRF3 mutants, we showed that PSMD14 could strongly bind to WT IRF3 and its 5A mutant, but not the 5D mutant (Figure 5H). We next investigated the K27-linked ubiquitination of IRF3 mutants after SeV infection. The IRF3-5D mutant exhibited a higher ubiquitination level of IRF3 compared with WT and 5A mutants of IRF3, and *PSMD14* knockdown only led to the enhancement of the ubiquitination of WT IRF3 and IRF3-5A mutant (Figure 5I). On the contrary, overexpression of PSMD14 could deubiquitinate WT IRF3 and the IRF3-5A mutant, but not the IRF3-5D mutant (Figure S5C). These results indicated that PSMD14 was more likely to remove the K27-linked ubiquitin chains from the inactive form of IRF3.

We subsequently detected the interaction between CALCOCO2 and different mutants of IRF3. Consistently, our results revealed that 5A mutant of IRF3 showed a low affinity to CALCOCO2, while 5D mutant of IRF3 displayed a higher affinity to CALCOCO2 even without viral infection (Figure 5J). The IRF3-5D mutant exhibited a higher degradation rate than that of WT IRF3 (Figure S5D). Together, our results revealed that PSMD14 failed to protect the active IRF3 from CALCOCO2-dependent autophagic degradation; thus, CALCOCO2-mediated selective autophagy could shut down the excessive activation of type I IFN signaling by degrading active IRF3.

PSMD14 increases the antiviral immune responses in human cells

Since PSMD14 promoted the stabilization of IRF3, we next investigated whether PSMD14 acts as a positive regulator of antiviral immunity. IFN-stimulated response element (ISRE)-driven luciferase reporter assay showed that knockout of *PSMD14* impaired type I IFN signaling activation induced by SeV and IC poly(I:C) (Figure 6A and S6A). We also found that *PSMD14* deficiency inhibited both DDX58 (N) and CGAS-STING-triggered IFN induction (Figure S6A), indicating that PSMD14 was involved in both RNA and DNA virus-induced type I IFN signaling pathways. We further showed that *PSMD14* deficiency decreased the release of IFNB1, as well as its downstream IFN stimulated genes (ISGs), in A549 cells (Figure 6B, S6B and S6C). Consistent with these results, we observed that *PSMD14* deficiency downregulated both the production of IFNB1 and the transcription of *IFNB1* in PBMCs (Figure 6C and S6D). Similarly, knockdown of *PSMD14* markedly reduced the phosphorylation level of IRF3 and STAT1 after SeV infection, but barely affected the phosphorylation of TBK1 (Figure 6D). In addition, *PSMD14* deficiency also reduced the dimerization of IRF3 as well as the translocation of IRF3 from cytosol to nucleus (Figure 6D and S6E). Together, our results suggested that PSMD14 functioned as a positive regulator of IRF3-mediated type I IFN signaling.

To characterize the function of PSMD14 in viral infection, we also performed real time-PCR analysis to confirm that the replication of SeV was increased in *PSMD14* KO A549 cells (Figure S6F). Consistently, knockdown of *PSMD14* significantly potentiated the replication of SeV in PBMCs (Figure 6E). We next overexpressed $IRF3^{K313\ R}$ in *IRF3* KO cells and found that PSMD14 lost its function in potentiating type I IFN signaling (Figure 6F). PSMD14 failed to promote the induction of IFNB1 in *CALCOCO2* KO cells, but not *SQSTM1* KO cells (Figure 6G). Moreover, *PSMD14* knockdown could barely affect the IFN signaling in mouse cells. However, PSMD14 regained its ability to facilitate the IFN signaling as well as to restrict viral replication in RAW264.7 cells reconstituted with human CALCOCO2 (Figure 6H, S6G,H). Together, these results reveal that PSMD14 functions as a positive regulator in type I IFN signaling as well as innate antiviral immunity in human cells.

Discussion

Autophagy is a conserved degradation pathway that disassembles and recycles dysfunctional cellular components. Accumulating evidence has revealed the crosstalk between autophagy and immune responses [2,35]. Several key molecules in autophagy, such as ATG16L1, ATG12–ATG5, BECN1, ULK1 and ATG9, are reported to directly regulate type I IFN antiviral responses [41–45]. In addition to regulating the type I IFN signaling pathway in an autophagic degradation-independent manner, autophagy is also reported to selectively degrade key immune factors in type I IFN signaling. LRRC25, BST2-MARCHF8, RNF34 and TRIM32 promote the degradation of DDX58, MAVS, and TICAM1 through autophagy cargo receptor SQSTM1, CALCOCO2, and TAX1BP1, respectively [24,25,46,47]. Moreover, both CGAS and STING1 are ubiquitinated after activation and are delivered to autophagosomes for degradation by SQSTM1 [23,26]. It has been reported that TRIM21 acts as a platform for the degradation of active IRF3 [19]. However, the mechanism underlying the autophagic degradation of IRF3 remains unclear. Here, we found that viral infection promotes K27-linked ubiquitination of IRF3. Subsequently, the cargo receptor CALCOCO2 recognizes the K27-linked ubiquitination of IRF3 and facilitates the autophagic degradation of IRF3, which contributes to the immune suppression of type I IFN signaling. Interestingly, CALCOCO2 is specifically involved in the regulation of the autophagic degradation of IRF3 in human cells. Lacking the ubiquitin-binding domain LIM-L, murine CALCOCO2 exhibits distinct function compared with its human homolog in regulating the stabilization of IRF3 and the activation of type I IFN signaling [25,34]. It is also worth reminding that both CALCOCO2 and SQSTM1 could interact with IRF3, and SQSTM1 might also play a role in control IRF3 stability under other conditions. Moreover, $IRF3^{K313\ R}$, which impairs the K27-linked ubiquitination on IRF3, still has a weak interaction with CALCOCO2. These results suggested that CALCOCO2 might bind to IRF3 via

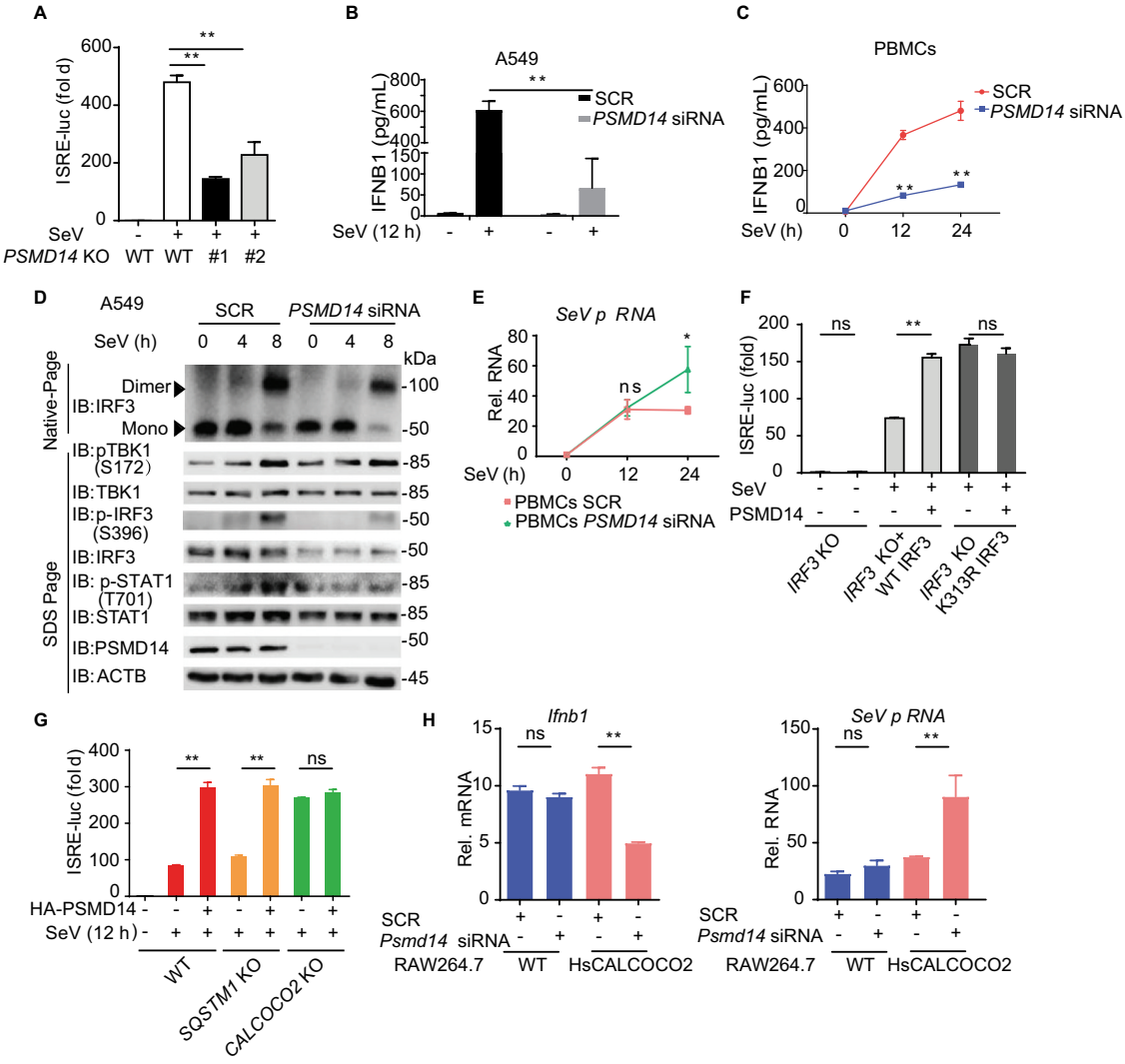

Figure 6. PSMD14 increases the antiviral immune responses. (A) Luciferase activity of *PSMD14* knockout (KO) 293 T cells transfected with an ISRE promoter-driven luciferase reporter after SeV infected for 18 h. (B) Enzyme-linked immunosorbent assay analysis (ELISA) of IFNB1 in the supernatants of A549 cells transfected with scramble (SCR) siRNA or *PSMD14*-specific siRNA, followed with or without SeV infection (MOI = 0.1). (C) PBMCs transfected with SCR or *PSMD14*-specific siRNA were infected with SeV (MOI = 1) at different time points. Relative expression level of IFNB1 in the supernatants was measured by ELISA. (D) A549 cells were transfected with SCR or *PSMD14*-specific siRNA, followed by treatment with SeV (MOI = 0.1) at different time points, the lysates were analyzed with indicated antibodies. (E) PBMCs transfected with SCR or *PSMD14*-specific siRNA were infected with SeV (MOI = 0.1) at different time points. Relative RNA level of *SeV phosphoprotein* was measured by real-time PCR. (F) Lysates of *IRF3* KO 293 T cells transfected with the ISRE luciferase reporter, together with empty vector or HA-PSMD14, plus the expression vector for Flag-IRF3, followed by SeV infection for indicating time points were used for luciferase assay. (G) Lysates of wild-type (WT), *SQSTM1*, and *CALCOCO2* KO 293 T cells transfected with the ISRE luciferase reporter, together with empty vector or HA-PSMD14, followed by SeV infection for indicating time points were used for luciferase assay. (H) RAW264.7 cells stably expressing human CALCOCO2 (HsCALCOCO2) were transfected with SCR or *Psmd14*-specific siRNAs, the expression of *Ifnb1* and replication of SeV were analyzed by real-time PCR. Data in (A-C) and (E-H) are expressed as mean ± SEM of three independent experiments. *$p < 0.05$, **$p < 0.01$; NS, not significant (two-tailed Student's *t*-test). All other experiments are representatives of three independent biological experiments with similar results.

a K27-linked ubiquitination-independent manner through other unknown mechanisms.

The post-translational modification of IRF3 plays a critical role in determining the immune state and the cell fate against viral infection. In the unstimulated state, IRF3 resides in the cytoplasm. Upon viral infection, IRF3 is phosphorylated at specific serine residues in the auto-inhibitory region, which allows its dimerization and nuclear translocation to initiate the IFN signaling. In our study, we reveal that the active form of IRF3 can also undergo ubiquitination, which leads to the degradation of IRF3 and results in immune suppression to avoid excessive IFN activation. Moreover, previous studies also revealed that higher concentration of viral infection could also contribute to the linear polyubiquitination on IRF3 and initiates the RIPA pro-apoptotic antiviral pathway for apoptotic cell death [8], which indicates the critical roles of IRF3 in mediating the transition of different kinds of immune responses.

In our previous study, we identified a large portion of DUBs as negative regulators in modulating the type I IFN-mediated antiviral response [37]. Here, we demonstrated that another DUB, PSMD14 could remove the K27-linked ubiquitination of IRF3 and reverse the autophagic degradation of IRF3; thus, positively regulating type I IFN signaling. In the unstimulated cells, PSMD14 associates with the latent form of IRF3 in the cytosol and deubiquitinates IRF3, which ensures

the basal level of IRF3 to maintain the adequate immune response after viral infection.

During viral infection, the accumulation of virus not only leads to the phosphorylation and conformational change of IRF3, but also results in the release of PSMD14 from IRF3 complex and the recruitment of E3 ligases, such as TRIM21, to the IRF3 complex, leading to the ubiquitination of IRF3. The ubiquitinated IRF3 undergoes degradation, and thus reducing the type I IFN signaling to avoid excessive detrimental production of downstream cytokines (Figure 7). We also showed that PSMD14 fails to promote the stabilization of IRF3 in RAW264.7 cells, while overexpression of human CALCOCO2 can restore the function of PSMD14 in RAW264.7 cells, indicating that the distinct regulatory functions of human and murine PSMD14 in type I IFN production may be due to the evolutionary selection in LIM-L domain of CALCOCO2.

Together, in this study, we identified PSMD14 as a DUB to remove the K27-linked ubiquitin chains on IRF3 and inhibit the CALCOCO2-mediated autophagic degradation of IRF3, thus ensuring the basal level of IRF3 to initiate the proper immune responses against viral infection. We also illustrated that the degradation of IRF3 mediated by selective autophagy triggers the immune suppression to avoid excessive activation of IFN signaling. Given the importance of IRF3 in activating type I IFN signaling and other key signaling pathways during viral infection, our finding expands our understanding of IRF3 activation and regulation in antiviral immunity and the development of therapeutic interventions approach by precisely controlling the immune suppression.

Materials and methods

Cell lines and culture conditions

HEK293 T (ATCC, CRL-11,268), HeLa (ATCC, CCL-2), A549 (ATCC, CCL-185), RAW264.7 cells (ATCC, TIB-71), and MEFs (ATCC, SCRC-1008) were cultured in DMEM medium (Gibco, 10,566,016) with 10% (vol:vol) fetal bovine serum (Gibco, 10,270,160) and 1% glutamine (Gibco, 25,030,081). PBMCs and THP-1 cells (ATCC, TIB-202) were maintained in RPMI-1640 medium (Gibco, 11,875–085) 10% fetal bovine serum. To induce starvation, cells were washed with phosphate-buffered saline (PBS; Gibco, 10,010,049) and incubated in EBSS (Gibco, 24,010,043). All cells were incubated in a 37° C incubator with 5% CO_2.

Plasmids and siRNA transfection

Constructs coding for PSMD14 and its point mutant were cloned in the pcDNA3.1 vector (provided by Rongfu Wang laboratory) for transient expression and into the FG-EH-DEST vector (provided by Xiaofeng Qin laboratory) for retroviral expression. 293 T transfection was performed using Lipofectamine 2000 (Invitrogen, 11,668,030) according to procedures recommended by the manufacturer. Chemically synthesized 21-nucleotide siRNA duplexes were obtained from TranSheepBio and transfected using Lipofectamine RNAiMAX (Invitrogen, 13,778,150) according to the manufacturer's instructions.

Generation of stable expression and knockout cell lines

The retroviral vectors (15 μg) were co-transfected with 5 μg of an expression plasmid for the vesicular stomatitis virus G protein into the 293 T cell line. The medium was changed the following day and the viral containing supernatant was collected 48 h after transfection, filtered through a 0.45 mm filter and subsequently used to infect cells with Polybrene (8 μg ml^{-1}). A549 cells were infected by incubation with retrovirus-containing supernatant for 48 h. For *PSMD14* KO cells, target sequences were cloned into pLentiCRISPRv2

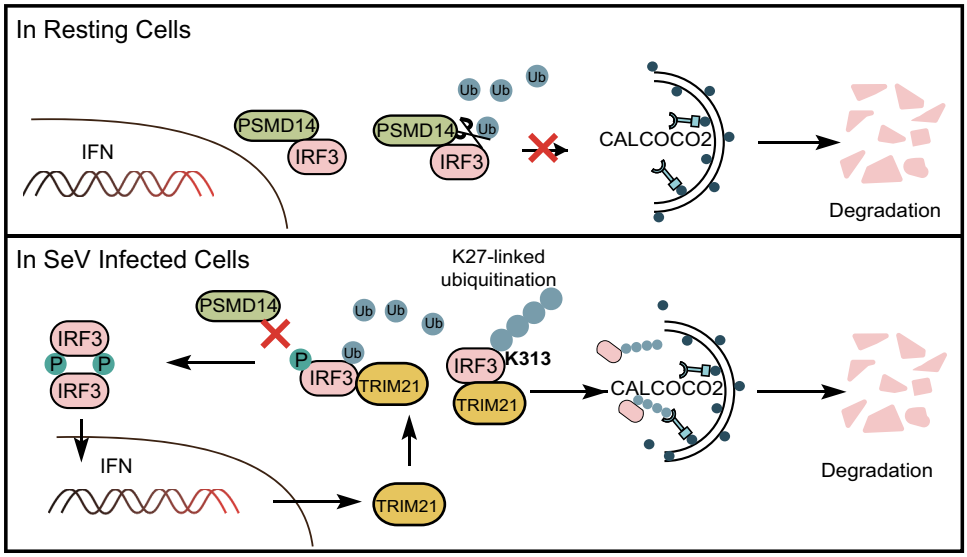

Figure 7. The working model of the precise regulation of IRF3 activity mediated by PSMD14 and CALCOCO2.

(Addgene, 52,961) by cutting with BsmBI. Transduced cells were purified by puromycin selection.

Quantitative RT-PCR

Total RNA was extracted from cells using the Trizol reagent (Invitrogen, 10,296,010) according to the manufacturer's instructions. For RT-PCR analysis, cDNA was generated with HiScript® II Q RT SuperMix for qPCR (+gDNA wiper) (Vazyme, R223-01) and was analyzed by quantitative real-time PCR using the 2× RealStar Green Power Mixture (GenStar, A301). All data were normalized to *Gapdh* expression.

Immunoprecipitation and immunoblot analysis

For immunoprecipitation, whole-cell extracts were prepared after transfection or stimulation with appropriate ligands, followed by incubation overnight with the appropriate antibodies plus Protein A/G beads (Pierce, 20,423). For immunoprecipitation with anti-Flag or anti-hemagglutinin, anti-Flag agarose gels (Sigma, A2220) were used. Beads were then washed five times with low-salt lysis buffer (50 mM HEPES [Gibco, 15,630,080], 150 mM NaCl, 1 mM EDTA [Vetec, V900106], 10% glycerol [Thermo Scientific, 17,904], 1.5 mM $MgCl_2$, and 1% Triton X-100 [Invitrogen, HFH10]), and immunoprecipitates were eluted with 2 × SDS Loading Buffer and resolved by SDS-PAGE. Proteins were transferred to PVDF membranes (Bio-Rad, 1,620,177) and further incubated with the appropriate antibodies. Immobilon Western Chemiluminescent HRP Substrate (Millipore, WBKLS0500) was used for protein detection. The information of the antibodies used in this study were listed in Table S1.

Protein purification

Recombinant His-tagged proteins were expressed and purified from *E. coli* strain BL21 (Thermo Scientific, EC0114). Cells were resuspended in His-lysis buffer (50 mM Tris-HCl pH 7.9, 150 mM NaCl, 1% Triton X-100, 2 mM DTT [Sigma, 10,197,777,001], 20 mM imidazole [Sigma, 56,750], and protease inhibitors [Roche, 11,697,498,001]) and lysed by sonication. After centrifugation and filtration, the extract was loaded onto Ni-NTA Columns (Thermo, R90110). After washing with lysis buffer for 5 times, the protein was eluted using lysis buffer containing 400 mM imidazole. The eluted proteins were dialyzed into TBS buffer (50 mM Tris-HCl pH 7.9, 150 mM NaCl, 5% glycerol and 3 mM beta-mercaptoethanol [Sigma, M3148]). For purification of proteins from HEK293 cells, MYC-PSMD14 and Flag-IRF3 were expressed by transient transfection and cells were harvested in low-salt lysis buffer. The lysates were incubated with Anti-MYC Agarose Affinity Gel (Thermo, 20,168) or ANTI-FLAG M2 Affinity Gel (Sigma, A2220) after clearing the lysate by centrifugation. The bound material was eluted using lysis buffer containing 0.5 mg/mL 3 × FLAG Peptide (APEX Bio, A6001) or 0.5 mg/ml MYC peptide (APEX Bio, A6003).

In vivo and in vitro deubiquitination assay

For *in vivo* deubiquitination assays in cultured cells, the cells were lysed with low-salt lysis buffer and the supernatants were denatured at 95°C for 5 min in the presence of 1% SDS. The denatured lysates were diluted with low-salt lysis buffer to reduce the concentration of SDS below 0.1%, followed by immunoprecipitation (denature-IP) with the indicated antibodies. The immunoprecipitates were subjected to immunoblot analysis with indicated antibodies. For *in vitro* deubiquitination assays, ubiquitinated IRF3 was isolated from 293 T cells transfected with expression vectors for HA-K27 Ub and Flag-IRF3. The cells were lysed with low-salt lysis and the supernatants were denatured at 95°C for 5 min in the presence of 1% SDS. Ubiquitinated IRF3 was diluted and purified from the cell extracts with anti-Flag affinity column in Flag-lysis buffer (50 mM Tris-HCl [pH 7.8], 137 mM NaCl, 10 mM NaF [Sigma, S7920], 1 mM EDTA, 1% Triton X-100, 0.2% Sarcosyl [Sigma, L5125], 1 mM DTT, 10% glycerol and fresh proteinase inhibitors). After extensive washing with the Flag-lysis buffer, the proteins were eluted with 3 × FLAG Peptide (APEX Bio, A6001). Ubiquitinated IRF3 protein was incubated with recombinant PSMD14 or its mutants in the deubiquitination buffer (50 mM Tris-HCl [pH 8.0], 50 mM NaCl, 1 mM EDTA, 10 mM DTT, 5% glycerol) for 2 h at 37°C.

Luciferase and reporter assays

293 T (2×10^5) cells were plated in 24-well plates and transfected using Lipofectamine 2000, with plasmids encoding an ISRE or IFNB1 luciferase reporter (firefly luciferase; 100 ng) and pRL-TK (renilla luciferase plasmid; 10 ng; provided by Rong-Fu Wang laboratory) together with 100 ng plasmid encoding Flag-DDX58 (N), Flag-cGAS, Flag-STING, Flag-IFIH1, Flag-MAVS, Flag-TBK1, Flag-IKKi, or Flag-IRF3 (5D) (provided by Rong-Fu Wang laboratory) and increasing concentrations (0, 100, or 200 ng) of plasmids expressing PSMD14. Empty pcDNA3.1 vector (provided by Rong-Fu Wang laboratory) was used to maintain equal amounts of DNA among wells. Then, the cells were infected with SeV for indicated time points. Cells were collected and luciferase activity was measured with the Dual-Luciferase Assay (Promega, E1910) with a Luminoskan Ascent luminometer (Thermo Fisher Scientific, 2,805,621), according to the manufacturer's protocol. Reporter gene activity was determined by normalization of the firefly luciferase activity to renilla luciferase activity.

Fluorescence microscopy

Cells were cultured on Glass Bottom culture dishes (Nest Scientific) and directly observed as previously described [23]. For examination by immunofluorescence microscopy, cells were fixed with 4% paraformaldehyde for 15 min, and then permeabilized in methyl alcohol for 10 min at −20°C. After washing with PBS for 3 times, cells were blocked in 5% fetal goat serum (Boster Biological, AR1009) for 1 h, and then incubated with primary antibodies diluted in 10% bull

serum albumin (Sigma, A1933) overnight. The cells were washed and followed by a fluorescently labeled secondary antibody (CF568 goat anti-mouse IgG [H + L] and Alexa Fluor 488 conjugated anti-rabbit-IgG). Confocal images were examined using a microscope (LSM710; Carl Zeiss) equipped with 100 × 1.40 NA oil objectives, with Immersol 518 F (Carl Zeiss) as imaging medium and a camera (AxioCam HRc; Carl Zeiss) under the control of Zen 2008 software (Carl Zeiss). The images were processed for gamma adjustments using LSM Zen 2008 or ImageJ software (National Institutes of Health).

Virus infection

Sendai virus were kindly provided by Dr. Xiaofeng Qin (Suzhou Institute of Systems Medicine). Cells were infected at various MOI, as previously described [23,25].

Quantification and statistical analysis

Data are represented as mean ± SEM unless otherwise indicated, and Student's *t*-test was used for all statistical analysis with the GraphPad Prism 5 software. Differences between two groups were considered significant when *P* value was less than 0.05.

Acknowledgments

We are grateful to Jiang Li, and Daijia Huang (Sun Yat-sen University Cancer Center) for the kind gift of PBMCs.

Disclosure statement

The authors declare no competing interests.

Funding

This work was supported by National Natural Science Foundation of China [31870862, 31700760, 31970700, and 31800751], Science and Technology Planning Project of Guangzhou, China [201804010385], National Key Basic Research Program of China [2015CB554301], and the Fundamental Research Funds for the Central Universities [18lgpy49 and 18lgpy53].

ORCID

Jun Cui http://orcid.org/0000-0002-8000-3708

References

[1] Liu J, Qian C, Cao XT. Post-translational modification control of innate immunity. Immunity. 2016;45:15–30.
[2] Choi Y, Bowman JW, Jung JU. Autophagy during viral infection - a double-edged sword. Nat Rev Microbiol. 2018;16:340–353.
[3] Chan YK, Gack MU. Viral evasion of intracellular DNA and RNA sensing. Nat Rev Microbiol. 2016;14:360–373.
[4] Schlee M, Hartmann G. Discriminating self from non-self in nucleic acid sensing. Nat Rev Immunol. 2016;16:566–580.
[5] Taniguchi T, Ogasawara K, Takaoka A, et al. IRF family of transcription factors as regulators of host defense. Annu Rev Immunol. 2001;19:623–655.
[6] Lin R, Heylbroeck C, Pitha PM, et al. Virus-dependent phosphorylation of the IRF-3 transcription factor regulates nuclear translocation, transactivation potential, and proteasome-mediated degradation. Mol Cell Biol. 1998;18:2986–2996.
[7] Qin BY, Liu C, Lam SS, et al. Crystal structure of IRF-3 reveals mechanism of autoinhibition and virus-induced phosphoactivation. Nat Struct Biol. 2003;10:913–921.
[8] Chattopadhyay S, Kuzmanovic T, Zhang Y, et al. Ubiquitination of the transcription factor IRF-3 activates RIPA, the apoptotic pathway that protects mice from viral pathogenesis. Immunity. 2016;44:1151–1161.
[9] Tamura T, Yanai H, Savitsky D, et al. The IRF family transcription factors in immunity and oncogenesis. Annu Rev Immunol. 2008;26:535–584.
[10] Zhao X, Zhu H, Yu J, et al. c-Cbl-mediated ubiquitination of IRF3 negatively regulates IFN-beta production and cellular antiviral response. Cell Signal. 2016;28:1683–1693.
[11] Zhang M, Tian Y, Wang RP, et al. Negative feedback regulation of cellular antiviral signaling by RBCK1-mediated degradation of IRF3. Cell Res. 2008;18:1096–1104.
[12] Lei CQ, Zhang Y, Xia T, et al. FoxO1 negatively regulates cellular antiviral response by promoting degradation of IRF3. J Biol Chem. 2013;288:12596–12604.
[13] Higgs R, Ni Gabhann J, Ben Larbi N, et al. The E3 ubiquitin ligase Ro52 negatively regulates IFN-beta production post-pathogen recognition by polyubiquitin-mediated degradation of IRF3. J Iimmunol. 2008;181:1780–1786.
[14] Saitoh T, Tun-Kyi A, Ryo A, et al. Negative regulation of interferon-regulatory factor 3-dependent innate antiviral response by the prolyl isomerase Pin1. Nat Immunol. 2006;7:598–605.
[15 Mitoma H, Hanabuchi S, Kim T, et al. The DHX33 RNA helicase senses cytosolic RNA and activates the NLRP3 inflammasome. Immunity. 2013;39:123–135.
[16] Yu Y, Hayward GS. The ubiquitin E3 ligase RAUL negatively regulates type i interferon through ubiquitination of the transcription factors IRF7 and IRF3. Immunity. 2010;33:863–877.
[17] Zeng W, Xu M, Liu S, et al. Key role of Ubc5 and lysine-63 polyubiquitination in viral activation of IRF3. Mol Cell. 2009;36:315–325.
[18] Jiang LQ, Xia T, Hu YH, et al. IFITM3 inhibits virus-triggered induction of type I interferon by mediating autophagosome-dependent degradation of IRF3. Cell Mol Immunol. 2018;15:858–867.
[19] Kimura T, Jain A, Choi SW, et al. TRIM-mediated precision autophagy targets cytoplasmic regulators of innate immunity. J Cell Biol. 2015;210:973–989.
[20] Clarke AJ, Simon AK. Autophagy in the renewal, differentiation and homeostasis of immune cells. Nat Rev Immunol. 2019;19:170–183.
[21] Gatica D, Lahiri V, Klionsky DJ. Cargo recognition and degradation by selective autophagy. Nat Cell Biol. 2018;20:233–242.
[22] Dikic I, Elazar Z. Mechanism and medical implications of mammalian autophagy. Nat Rev Mol Cell Biol. 2018;19:349–364.
[23] Chen M, Meng Q, Qin Y, et al. TRIM14 inhibits cGAS degradation mediated by selective autophagy receptor p62 to promote innate immune responses. Mol Cell. 2016;64:105–119.
[24] Du Y, Duan T, Feng Y, et al. LRRC25 inhibits type I IFN signaling by targeting ISG15-associated RIG-I for autophagic degradation. Embo J. 2018;37:351–366.
[25] Jin S, Tian S, Luo M, et al. Tetherin suppresses type I interferon signaling by targeting MAVS for NDP52-mediated selective autophagic degradation in human cells. Mol Cell. 2017;68:308–22 e4.
[26] Prabakaran T, Bodda C, Krapp C, et al. Attenuation of cGAS-STING signaling is mediated by a p62/SQSTM1-dependent autophagy pathway activated by TBK1. Embo J. 2018;37:e97858.
[27] Liang XH, Yu J, Brown K, et al. Beclin 1 contains a leucine-rich nuclear export signal that is required for its autophagy and tumor suppressor function. Cancer Res. 2001;61:3443–3449.
[28] Choi AM, Ryter SW, Levine B. Autophagy in human health and disease. N Engl J Med. 2013;368:651–662.
[29] Green DR, Levine B. To be or not to be? How selective autophagy and cell death govern cell fate. Cell. 2014;157:65–75.

[30] Jo C, Gundemir S, Pritchard S, et al. Nrf2 reduces levels of phosphorylated tau protein by inducing autophagy adaptor protein NDP52. Nat Commun. 2014;5:3496.
[31] Thurston TL, Ryzhakov G, Bloor S, et al. The TBK1 adaptor and autophagy receptor NDP52 restricts the proliferation of ubiquitin-coated bacteria. Nat Immunol. 2009;10:1215–1221.
[32] Thurston TL, Boyle KB, Allen M, et al. Recruitment of TBK1 to cytosol-invading Salmonella induces WIPI2-dependent antibacterial autophagy. Embo J. 2016;35:1779–1792.
[33] Radivojac P, Vacic V, Haynes C, et al. Identification, analysis, and prediction of protein ubiquitination sites. Proteins. 2010;78:365–380.
[34] Deretic V, Saitoh T, Akira S. Autophagy in infection, inflammation and immunity. Nat Rev Immunol. 2013;13:722–737.
[35] Jin SH, Cui J. BST2 inhibits type I IFN (interferon) signaling by accelerating MAVS degradation through CALCOCO2-directed autophagy. Autophagy. 2018;14:171–172.
[36] Long L, Deng Y, Yao F, et al. Recruitment of phosphatase PP2A by RACK1 adaptor protein deactivates transcription factor IRF3 and limits type I interferon signaling. Immunity. 2014;40:515–529.
[37] Liu Q, Wu Y, Qin Y, et al. Broad and diverse mechanisms used by deubiquitinase family members in regulating the type I interferon signaling pathway during antiviral responses. Sci Adv. 2018;4:eaar2824.
[38] Lin H, Jiang M, Liu L, et al. The long noncoding RNA Lnczc3h7a promotes a TRIM25-mediated RIG-I antiviral innate immune response. Nat Immunol. 2019;20(7):812–823..
[39] Servant MJ, Grandvaux N, tenOever BR, et al. Identification of the minimal phosphoacceptor site required for in vivo activation of interferon regulatory factor 3 in response to virus and double-stranded RNA. J Biol Chem. 2003;278:9441–9447.
[40] Mori M, Yoneyama M, Ito T, et al. Identification of Ser-386 of interferon regulatory factor 3 as critical target for inducible phosphorylation that determines activation. J Biol Chem. 2004;279:9698–9702.
[41] Cadwell K. Crosstalk between autophagy and inflammatory signalling pathways: balancing defence and homeostasis. Nat Rev Immunol. 2016;16:661–675.
[42] Lei Y, Wen H, Yu Y, et al. The mitochondrial proteins NLRX1 and TUFM form a complex that regulates type I interferon and autophagy. Immunity. 2012;36:933–946.
[43] Jounai N, Takeshita F, Kobiyama K, et al. The Atg5 Atg12 conjugate associates with innate antiviral immune responses. Proc Natl Acad Sci U S A. 2007;104:14050–14055.
[44] Jin SH, Tian S, Chen YM, et al. USP19 modulates autophagy and antiviral immune responses by deubiquitinating Beclin-1. Embo J. 2016;35:866–880.
[45] Cui J, Jin SH, Wang RF. The BECN1-USP19 axis plays a role in the crosstalk between autophagy and antiviral immune responses. Autophagy. 2016;12:1210–1211.
[46] Yang Q, Liu TT, Lin H, et al. TRIM32-TAX1BP1-dependent selective autophagic degradation of TRIF negatively regulates TLR3/4--mediated innate immune responses. PLoS Pathog. 2017;13:e1006600.
[47] He X, Zhu Y, Zhang Y, et al. RNF34 functions in immunity and selective mitophagy by targeting MAVS for autophagic degradation. Embo J. 2019;38:e100978.